



Effect of OH, NH₂ and OCH₃ groups on the corrosion inhibition efficacy of three new 2,4,5-trisubstituted imidazole derivatives on mild steel in acidic solutions: Experimental, surface and DFT explorations

M.K. Prashanth^a, C.B. Pradeep Kumar^{b,*}, B.S. Prathibha^a, M.S. Raghu^c, K. Yogesh Kumar^d, M.B. Jagadeesha^b, K.N. Mohana^e, Honnur Krishna^f

^a Dept of Chemistry, BNM Institute of Technology, Bangalore 560070, India

^b Dept of Chemistry, Malnad College of Engineering, Hassan 573202, India

^c Dept of Chemistry, New Horizon College of Engineering, Bangalore 560103, India

^d Department of Chemistry, Jain University, Ramanagara, 562112, Bangalore, India

^e Dept of Studies in Chemistry, University of Mysore, Manasagangothri, Mysuru 570006, India

^f Department of Chemistry, S.D.V.S. Sangh's S. S. Arts College T.P. Science Institute, Sankeshwar, Belagavi, Karnataka 591313, India

ARTICLE INFO

Article history:

Received 16 December 2020

Received in revised form 27 January 2021

Accepted 2 February 2021

Available online 5 February 2021

Keywords:

Mild steel

Imidazoles

Electrochemical impedance spectroscopy

SEM

XPS

DFT

QC

ABSTRACT

Three new imidazole derivatives namely, 4-(4,5-bis(4-methoxyphenyl)-1H-imidazol-2-yl)phenol (IM₁), 4-(4,5-bis(4-methoxyphenyl)-1H-imidazol-2-yl)benzenamine (IM₂), 2,4,5-tris(4-methoxyphenyl)-1H-imidazole (IM₃) were synthesized using microwave irradiation method. The noteworthy highlights of this method are safe reaction profiles, broad substrate scope, short run time, catalyst-free, excellent yields, economical, solvent-free, and simple workup conditions. The structural characterization of all the imidazole derivatives has been confirmed by ¹HNMR and mass spectral techniques. The corrosion inhibition potential of all the imidazoles was explored using weight loss and electrochemical methods. The imidazole derivative (IM₁) bearing a hydroxyl group exhibited maximum corrosion inhibition efficiency compared to other imidazoles (up to 96%). Strong adsorption of studied imidazole molecules followed the Langmuir model with very good correlation coefficients. The calculated Gibbs free energy of adsorption values suggested the mixed type of adsorption (physisorption and chemisorption). The polarization measurements indicated studied imidazole derivatives as mixed types of corrosion inhibitors. Further, scanning electron microscopy (SEM), XPS and XRD were performed to study the surface morphology of Mild steel (MS) surface. Quantum chemical calculations (DFT) was used to prove the obtained inhibition efficiencies (η %).

© 2021 Elsevier B.V. All rights reserved.

1. Introduction

The study of corrosion and its inhibition is currently one of the most active fields to protect metals from various corrosive environments [1–3]. Mild steel (MS) is widely used in many industries because of its excellent structural and mechanical properties. MS also has many drawbacks i.e., degradation and corrosion in various acidic environments. However different acidic and basic solutions are extensively used in many chemical and petrochemical industries for effective acid pickling treatment. The major consequence of the pickling process is in addition to removing unwanted scales, acids cause significant damage to MS substrate. Hence, the demand for reducing the rate of corrosion and method development for the prevention of corrosion is high across the globe.

Metals destruction can be lowered by using many methods. Using a small amount of organic compounds as inhibitors is a method exhibit desirable practical application through which the rate of corrosion can be controlled. Generally, organic compounds containing π - electrons (N, S, and O) and different hetero atoms acts as efficient inhibitors in different aggressive solutions because of their strong adsorptive ability on the metal surface [4].

Several authors reported many organic compounds as corrosion inhibitors in different environments [5–9]. Studies have also demonstrated the rate of corrosion can be prevented by forming donor-acceptor complexes of inhibitor and metal surface. Thus, corrosion protection efficiency is directly proportional to functional groups, electron density, and electronic structure of inhibitor molecules [10–12]. In this connection, organic compounds containing imidazole moiety are the effective inhibitors for different metals in a different medium. Many imidazoles and its derivatives have been reported as excellent corrosion inhibitors in the different mediums [13–21]. Also, imidazole

* Corresponding author at: Dept of Chemistry, Malnad College of Engineering, Hassan 573202, India.

E-mail address: pradp12@gmail.com (C.B.P. Kumar).

Table 1
Optimization of reaction parameters.

Entry	NH ₄ OAc (mmol)	Temp (°C)	Time (min)	Yield (%)
1	1	100	5	63
2	1	100	8	68
3	1	100	10	72
4	1	110	10	76
5	1	120	10	77
6	2	100	5	71
7	2	100	8	79
8	2	100	10	84
9	2	110	10	93
10	2	110	12	93
11	2	120	10	93
12	3	110	10	93

contains 2 to 3 hetero atoms, therefore it is worth investigating the corrosion inhibition efficiency. Other important characteristic features of imidazole and its derivatives are low cost and low toxicity as reported in the literature [22]. For many years imidazole represents eco-friendly corrosion inhibitors for many substrates and belongs to the class of nitrogen-containing organic compounds with greater inhibition potential due to the high electron density around the nitrogen atoms [23].

A thought-provoking task has been the hunt for a creative key for the reduction reaction time, by products, workup procedure and increased yield in organic process. This can be resolved by carrying out the reaction in microwave condition. For accelerated organic synthesis, microwave-assisted synthesis has a significant effect on the synthetic organic chemist to prevent side product development. To date, numerous traditional methods for imidazole synthesis have been reported in the literature [24–28]. However, it was mentioned that all these approaches include several drawbacks such as tedious workup procedure, prolonged reaction time, poor yields, and use of expensive and environmentally toxic organic reagents or catalyst or solvent. We have therefore developed an ecofriendly, efficient, catalyst and solvent free method for the synthesis of imidazoles.

In the present work authors used three newly designed imidazole derivatives namely, 4-(4,5-bis(4-methoxyphenyl)-1H-imidazol-2-yl)phenol (IM₁), 4-(4,5-bis(4-methoxyphenyl)-1H-imidazol-2-yl)benzenamine (IM₂), 2,4,5-tris(4-methoxyphenyl)-1H-imidazole (IM₃) to evaluate corrosion inhibition efficiency on MS in HCl medium. To evaluate the inhibition efficiency both electrochemical (EIS & Potentiodynamic polarization) and gravimetric methods are used. Suitable adsorption isotherm was proposed, and thermodynamic parameters are calculated and reported. Surface morphology of MS surface (inhibited & uninhibited) has been evaluated using scanning electron microscopy (SEM), X-Ray Diffraction (XRD), and X-Ray photoelectron (XPS) techniques.

2. Experimental

2.1. Materials

The chemical composition of the studied MS coupon is as follows (wt%): Si-0.023, S- 0.023, C-0.051, Mn-0.179, Al-0.103, P 0.005, and

the remaining is iron. The specimens under study are abraded by using various grades SiC emery papers, then the MS specimen is washed with demineralized water and finally dried by using tissue paper after those MS specimens are immersed for 10 S in acetone and dried out later placed in desiccators. After the completion of weight loss experiments, the MS coupons were rinsed with acetone and weighed. Electrochemical measurements were performed by exposing an MS surface area of 1 cm³ (1 cm² surfaces was exposed by covering the MS surface by using epoxy resin). The calculated quantities of the imidazole derivatives were used to prepare the concentration of different inhibitors.

2.2. Synthesis of inhibitors

2.2.1. General procedure for the synthesis of 2,4,5-trisubstituted imidazole derivatives (3a-c)

The mixture of 4,4'-dimethoxybenzil (1 mmol), aromatic aldehyde (1 mmol), and ammonium acetate (2 mmol) were transferred to a clean and dry mortar, triturated to form a uniform mixture. The resulting mixture was then transferred to a 10 mL microwave vessel and it was heated at 110 °C using microwave irradiation (300 W) for 10 min. The reaction was monitored by TLC (hexane: ethyl acetate 7:3 v/v) and the products were allowed to cool to room temperature. The resulting residue was directly purified by column chromatography using hexane: ethyl acetate 7:3 v/v as eluent.

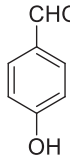
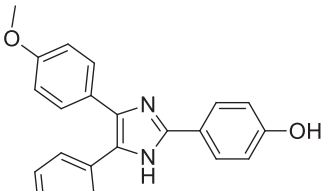
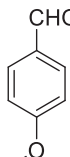
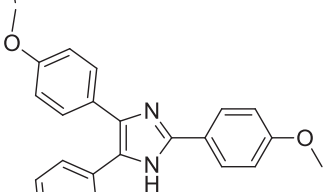
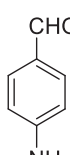
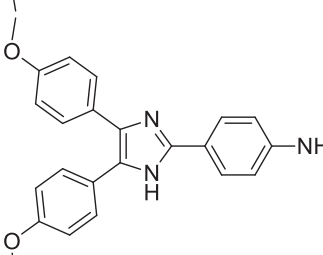
2.2.2. Synthesis of 4-(4,5-bis(4-methoxyphenyl)-1H-imidazol-2-yl)phenol (3a, IM₁)

mp.: 271 °C. Anal. calc. For C₂₃H₂₀N₂O₃: C, 74.18; H, 5.41; N, 7.52. found: C, 74.06; H, 5.35; N, 7.43. ¹H NMR (400 MHz, DMSO-*d*₆) δ: 3.73 (s, 6H, (-OCH₃)₂), 5.22 (s, 1H, -OH), 7.33–7.75 (m, 12H, Ar—H), 12.32 (s, 1H, -NH). MS, *m/z*: 373 (M + 1).

2.2.3. Synthesis of 4-(4,5-bis(4-methoxyphenyl)-1H-imidazol-2-yl)aniline (3b - IM₂)

mp.: 274 °C. Anal. calc. For C₂₃H₂₁N₃O₂: C, 74.37; H, 5.70; N, 11.31. found: C, 74.31; H, 5.62; N, 11.39. ¹H NMR (400 MHz, DMSO-*d*₆) δ: 3.73 (s, 6H, (-OCH₃)₂), 6.47 (s, 2H, -NH₂), 7.03–7.88 (m, 12H, Ar—H), 12.50 (s, 1H, -NH). MS, *m/z*: 372 (M + 1).

Table 2
Substrate scope of the reaction.

Compound	R	Product	Yield (%)
IM ₁ (3a)			93
IM ₂ (3b)			91
IM ₃ (3c)			90

2.2.4. Synthesis of 2,4,5-tris(4-methoxyphenyl)-1H-imidazole (3c)

mp.: 286 °C. Anal. calc. For C₂₄H₂₂N₂O₃: C, 74.59; H, 5.74; N, 7.25. found: C, 74.48; H, 5.69; N, 7.18. ¹H NMR (400 MHz, DMSO-*d*₆) δ: 3.76 (s, 9H, (-OCH₃)₃), 7.04–7.50 (m, 12H, Ar–H), 12.58 (s, 1H, -NH). MS, *m/z*: 387 (M + 1).

2.3. Methods

2.3.1. Electrochemical techniques

All the electrochemical evaluation was carried out in three-electrode systems namely, reference electrode (calomel), auxiliary (Pt), and working electrode (MS) in a CH1660D electrochemical workstation. Different concentrations of the imidazole derivatives were prepared and later evaluated for their electrochemical characteristics after immersing for 30 min at 30 °C. EIS analysis was carried out in 10.0 kHz to 0.1 Hz frequency range and at an amplitude of 0.005 V. A scan rate of 0.4 mV s⁻¹ was used at -200 to +200 mV potential range in potentiodynamic

polarization measurements. By using Tafel plots, the corrosion current density (*i*_{corr}) was evaluated.

2.3.2. Mass loss measurements

0.5 M HCl solution was used to immerse the 2 × 2 × 0.1 cm dimension MS sample. To this, different concentrations of the imidazole derivatives were added and after 6 h, the corrosion rate (*C*_R) and inhibition efficiency (*E*_{WL} %) are calculated using eqs. (1) and (2).

$$C_R = \frac{\Delta W}{S t} \quad (1)$$

$$E_{WL} \% = \frac{(C_R)_a - (C_R)_p}{(C_R)_a} \times 100 \quad (2)$$

where, (*C*_R)_a and (*C*_R)_p; corrosion rate in the absence and presence of inhibitors, *S*; surface area of the specimen (cm²), Δ*W*: weight loss, *t*; immersion time (h).

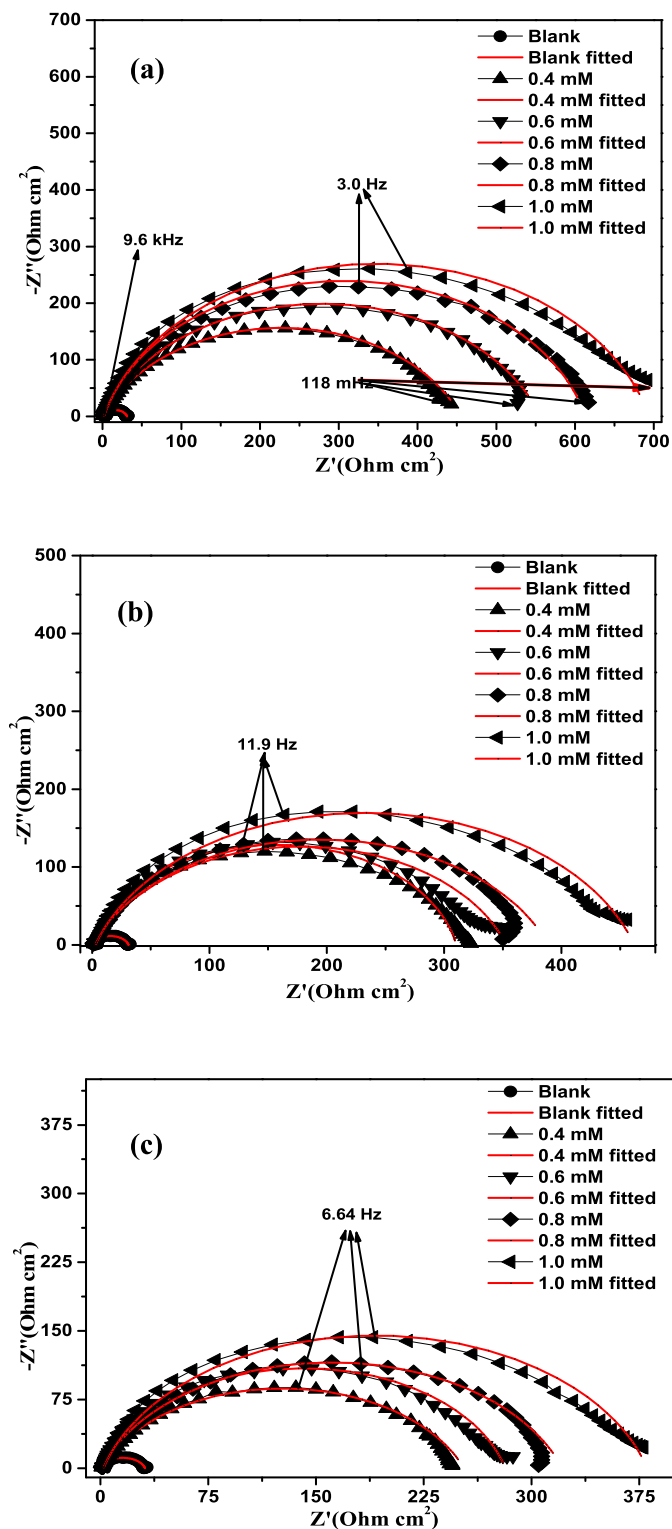


Fig. 1. Nyquist plots for MS in 0.5 M HCl solution containing different concentrations of (a) IM₁ (b) IM₂ (c) IM₃.

3. Results and discussion

3.1. Synthesis of imidazoles

Initially, to optimize the reaction conditions a model reaction was performed by the condensation of 4,4'-dimethoxybenzil (1 mmol) and 4-hydroxybenzaldehyde (1 mmol) under solvent-free conditions at

different temperature and various amounts of ammonium acetate as nitrogen source. The respective results are summarized in Table 1. After performing the test reaction at different temperatures (100, 110 and 120 °C) and in a various amounts of ammonium acetate, the highest conversion was obtained when the reaction mixture was irradiated at 300 W and 110 °C with the concentration of 2 mmol of ammonium

Table 3
Electrochemical impedance parameters for MS in 0.5 M HCl in the absence and presence of different concentrations of IM₁, IM₂ and IM₃.

Inhibitor	C (mM)	CPE _{film}			CPE _{dl}			R _p	C _{dl} (F cm ⁻²)	IE%
		Y _o (μ Ω ⁻¹ s ⁿ)	n ₁	R _{film}	Y _o (μ Ω ⁻¹ s ⁿ)	n ₂	R _{ct}			
IM ₁	0	0.000087	0.8169	5.14 ± 0.21	0.000016	1.000	25.1 ± 0.19	30	0.000016	
	0.4	0.0002001	0.8000	0.14 ± 0.22	0.01143	0.8000	454 ± 0.11	454	0.01725	93
	0.6	0.0000082	1.0000	1.87 ± 0.11	0.001487	0.7886	544 ± 0.14	555	0.001412	94
	0.8	0.00009842	0.7650	2.56 ± 0.23	0.00003639	0.9361	617 ± 0.32	619	0.000028	95
	1.0	0.00008073	0.7734	5.90 ± 0.29	0.00002664	0.9927	675 ± 0.25	681	0.000025	96
IM ₂	0.4	0.00006787	0.9006	275 ± 0.15	0.001411	0.9244	40.1 ± 0.34	315	0.00132	90
	0.6	0.00008269	0.7309	10.7 ± 0.13	0.00002891	1.0000	326 ± 0.16	337	0.000028	91
	0.8	0.00007026	1.0000	2.40 ± 0.35	0.0001825	0.8136	368 ± 0.23	370	0.000098	92
	1.0	0.00006737	0.7519	10.3 ± 0.29	0.00002092	1.0000	434 ± 0.26	444	0.000020	93
	IM ₃	0.4	0.0001461	0.7679	7.0 ± 0.10	0.00003857	0.8795	239 ± 0.06	246	0.00002038
0.6		0.0001147	0.8000	0.0 ± 0.22	0.00000000	0.8000	280 ± 0.09	280	0.00004856	89
0.8		0.00007391	0.8422	2.2 ± 0.21	0.00012460	0.8047	311 ± 0.21	313	0.0000567	90
1.0		0.00008839	0.7539	6.6 ± 0.32	0.00002914	1.0000	364 ± 0.34	371	0.00002914	92

acetate in solvent-free conditions. Under optimized conditions, the generality and scope of this approach were assessed with a representative selection of 4,4'-dimethoxybenzil and various aromatic aldehydes. The findings are listed in Table 2.

3.2. Electrochemical impedance analysis (EIS)

The Nyquist plots for studied inhibitors (IM₁, IM₂ & IM₃) (Fig. 1a, b & 1c) are obtained by immersing the different concentrations in 0.5 M HCl for about 30 min. Inspections of the figures revealed that the shape of the Nyquist plots are semicircles indicating the charge transfer process is mainly responsible for the corrosion process [29,30]. The impedance circles are not perfect semicircles. The distorted semicircles may be due to the surface inhomogeneity and roughness of the MS electrode [31–33]. Different concentrations of the inhibitors were added and observed the enhancement in the diameter of the semicircle upon increasing the inhibitor concentration. This suggests strong adsorption of the imidazole derivatives on the MS surface by blocking the active sites. The semicircle size of the IM₁ with electron-donating group OH is greatest compare to other imidazole derivatives (IM₂ with OCH₃ and IM₃ with NH₂) indicating the presence of more electron-donating groups in the inhibitors enhances corrosion inhibition by preventing the rate of corrosion to a greater extent. From the Nyquist plots, we have selected a suitable equivalent circuit (R(Q(R(QR))) with two time constant (Fig. 3) and analyzed all the plots. To fit EIS data more accurately the constant phase element (CPE) has been replaced by the capacitance in the interface, where R_s is the solution resistance; R_f and CPE_f represent the resistance and capacitance of inhibitor film. R_{ct} and CPE_{dl} represent the charge transfer resistance and double layer capacitance. The calculated CPE_f, CPE_{dl}, C_{dl}, R_p and IE% from the Nyquist plots are depicted in Table 3. The capacitance in the double layer is replaced with a constant phase element (CPE) to minimize the deviation caused due to frequency dispersion [34]. In the process of dissolution of metals in different acidic media, replacement of R_{ct} by R_p gives better approximation as R_p contains other resistance along with R_{ct} such as film resistance (R_f), i.e., R_p = R_f + R_{ct} [35]. The n value is derived from the Bode plots and indicating the deviation from the ideal capacitive behavior. The broader nature of Bode plots at higher concentrations suggested an increase in adsorption of inhibitor molecules on the mild steel surface. The Z_{CPE}, double-layer capacitance (C_{dl}) and η (%) can be calculated using the following equations:

$$Z_{CPE} = Y_o^{-1} (i\omega)^{-n} \quad (3)$$

$$C_{dl} = (Y_o R_{ct}^{1-n})^{1/n} \quad (4)$$

$$E_{RP}\% = \frac{(R_p)_p - (R_p)_a}{(R_p)_p} \times 100 \quad (5)$$

Inspection of Table 3 reveals that increasing R_p values with increasing the inhibitors concentrations and R_p values reach 95, 93 and 92% for IM₁, IM₂ and IM₃, respectively at 1.0 mM concentration suggesting superior corrosion inhibition protection due to presence of electron-donating groups in the studied imidazole derivatives. The bodes plots (Fig. 2a, b & c) explores one-time constant behavior of investigated imidazole derivatives. The values of the phase angle for blank are lowest compare to different concentrations indicating corrosion of MS [36]. The impedance results support that greater inhibition efficiency of IM₁ with more electron-donating group (OH) has more absorption capability on MS surface compare to IM₂ with OCH₃ and IM₃ with NH₂ groups. Hammett equation generally represents the electron-donating and electron releasing capability of various functional groups. Hammett constant (σ) is one of the prominent parameters which describes the electron-donating and accepting tendency of different substituents. Hammett constant (σ) value of IM₁ and IM₂ is +0.12 (σ_m) and -0.37 (σ_p) and for IM₃ is -0.16 (σ_m) and -0.66 (σ_p). Positive sign of Hammett constant associated with electron-donating substituents causes increasing corrosion inhibition efficiency. Whereas negative values of Hammett constant are always associated with electron-withdrawing substituents [37].

3.3. Polarization studies

Fig. 4a, b & c depicts the potentiodynamic polarization plots of MS in the presence and absence of various concentrations of IM₁, IM₂ and IM₃. Cathodic Tafel slope (β_a), current density (i_{corr}) and anodic Tafel slope (β_c) were calculated by the Tafel extrapolation method and the results are displayed in Table 4. From the figures, a shift of anodic and cathodic branches of Tafel plots to lower current densities indicates mixed mode (suppression of anodic metal dissolution and cathodic hydrogen evolution reactions) of corrosion inhibition. Mixed type of corrosion inhibition is also confirmed by evaluating the corrosion potential (E_{corr}; not greater than 85 mV) in presence of IM₁, IM₂ and IM₃ and found [38].

From the Table 4, it is also confirmed that the sharp decrease in i_{corr} values in presence of different concentrations of the imidazole derivatives causing an increase in corrosion inhibition efficiency (η%) reaches up to 96% for IM₁, 94% for IM₂ and 93% for IM₃ at 1.0 mM. This data suggests the strong corrosion protection efficiency of studied imidazole derivatives. The protonated IM₁, IM₂ and IM₃ reacts with hydrogen ions and adsorb on the cathodic regions and retard the hydrogen evolution reaction mediated by H⁺ ions released by acids. Oxidation of iron generates Fe²⁺ at the anode and negative charge caused due to chloride

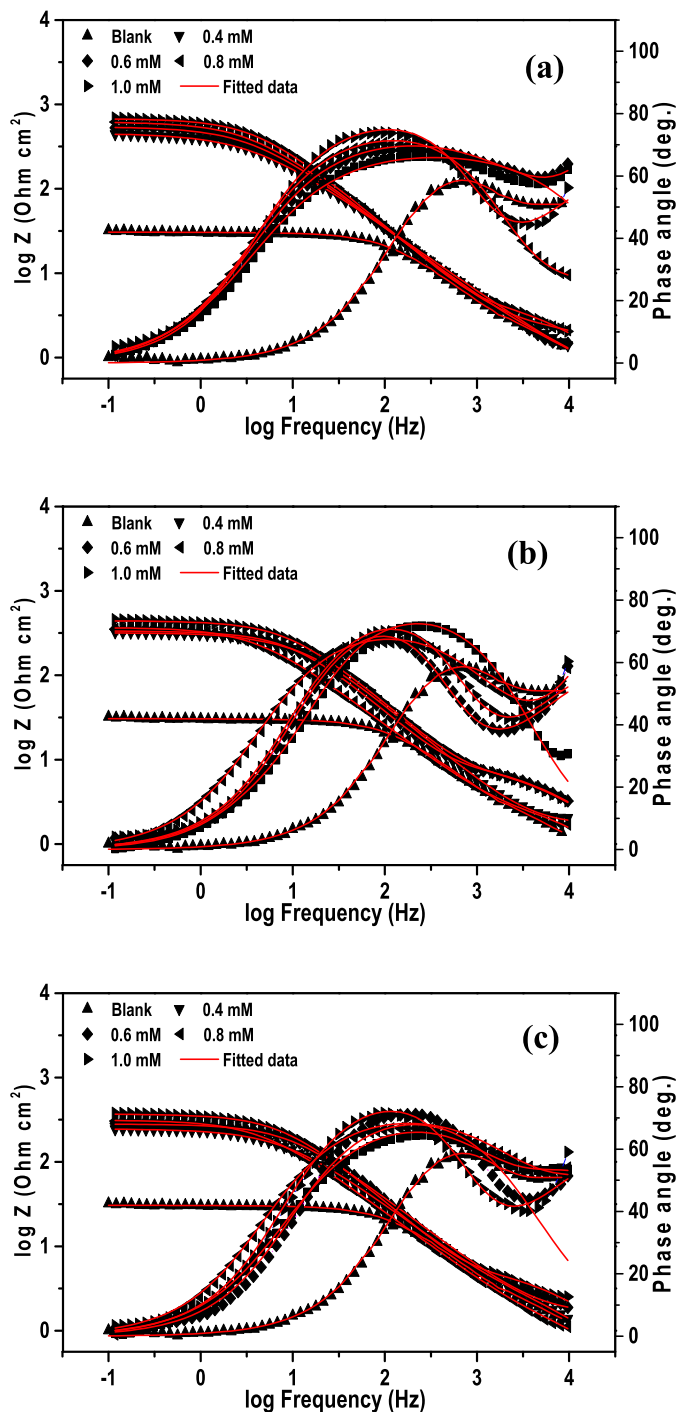


Fig. 2. Bodes plots for MS in 0.5 M HCl solution containing different concentrations of (a) IM₁ (b) IM₂ (c) IM₃.

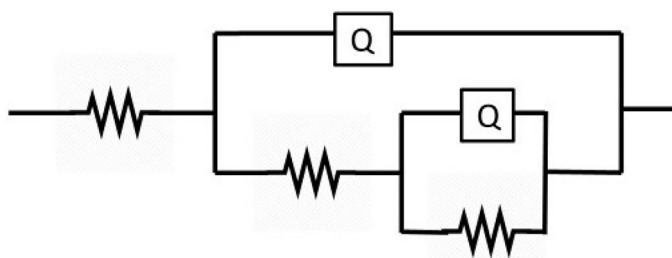


Fig. 3. Equivalent circuit diagram.

ions from hydrochloric acid would attracts IM₁, IM₂ and IM₃ for adsorption. Studied imidazole derivatives donate lone pair of electrons and benzene pi electrons to d orbitals of iron for effective adsorption. The $\eta\%$ follows the order IM₁ > IM₂ > M₃. The $\eta\%$ at various concentrations of imidazole derivatives are calculated using the eq. (6),

$$Ep\% = \frac{(i_{corr}^0) - (i_{corr}^i)}{(i_{corr}^0)} \times 100 \tag{6}$$

where, (i_{corr}^0) ; current density ($\mu\text{A cm}^{-2}$) for blank, (i_{corr}^i) ; current density ($\mu\text{A cm}^{-2}$) for inhibitors.

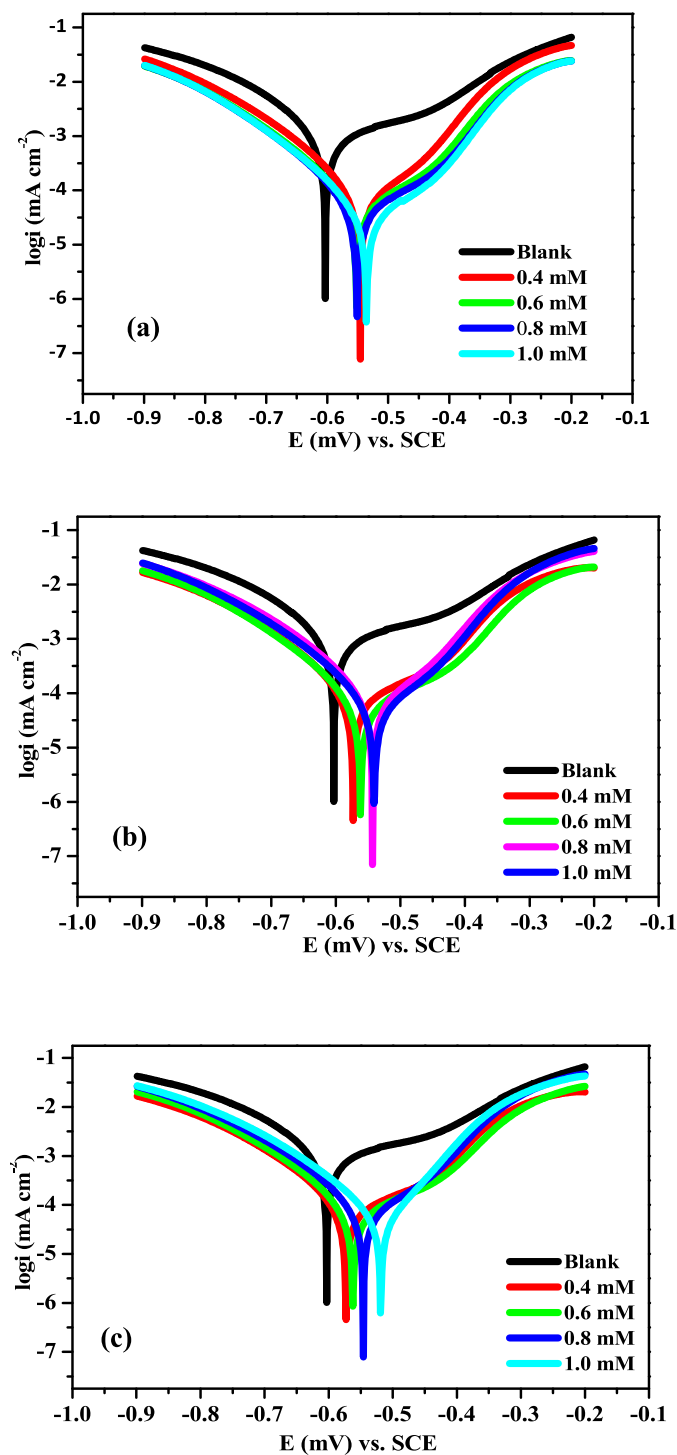


Fig. 4. Potentiodynamic polarization curves for MS in 0.5 M HCl solution containing different concentrations of (a) IM₁ (b) IM₂ (c) IM₃.

3.4. Weight loss studies

Table 5 depicts the calculated corrosion rate (C_R) and inhibition efficiency ($\eta\%$) values for 4,4'-dimethoxybenzil, 4-hydroxy benzaldehyde, 4-methoxy benzaldehyde, 4-Amino benzaldehyde and all the imidazole derivatives using weight loss measurements. Inhibition efficiency of starting compounds are relatively less comparing to other organic compounds. To achieve higher corrosion inhibition, we have synthesized IM₁, IM₂ and IM₃ and investigated their corrosion inhibition

efficiency. The mass loss studies have been carried out at 303 K for a period of 24 h. Results in the table indicate after the addition of IM₁, IM₂ and IM₃ corrosion rate decrease gradually indicating greater $\eta\%$ of investigated inhibitors. This could be attributed to the presence of π -electrons in the benzene ring as well as lone pair of electrons on the nitrogen atoms of the imidazole derivative which serve as a medium of adsorption [39].

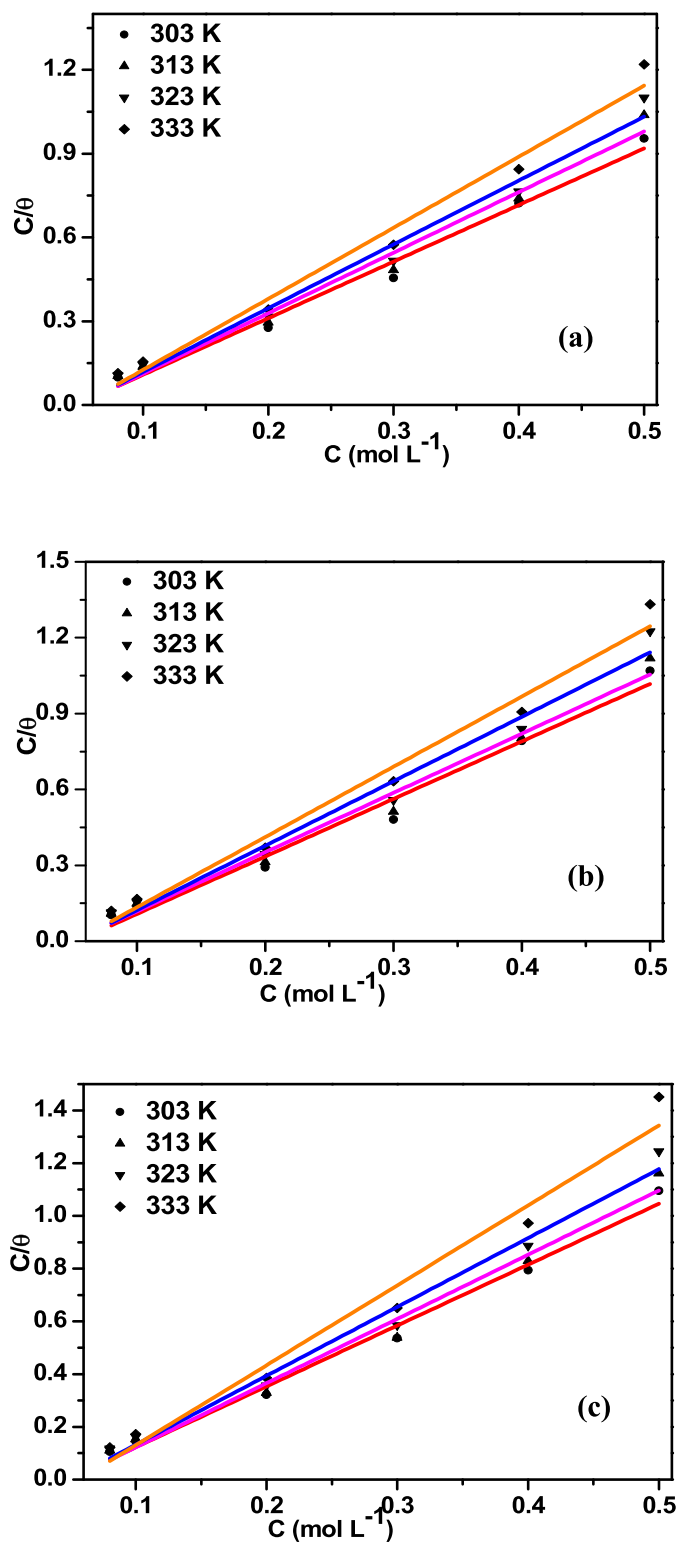
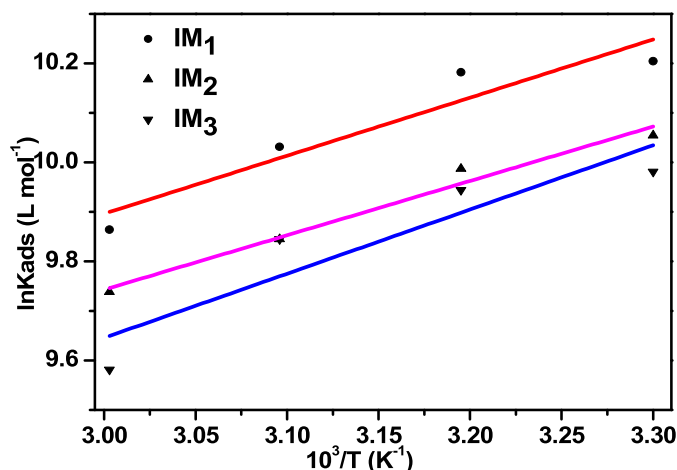


Fig. 5. Langmuir adsorption isotherm on MS in 0.5 M HCl at different temperatures (a) IM₁ (b) IM₂ (c) IM₃.

3.5. Adsorption studies

To establish the interaction between MS surface and IM₁, IM₂ and IM₃, various adsorption isotherm models were computed. These adsorption models include Langmuir, El -Awady, Frumkin, Temkin, Freundlich, and Flory -Huggins adsorption isotherms. Among various

isotherms the Langmuir isotherm model was best fitted with very good correlation coefficients (Very close to 1). Various adsorption thermodynamic parameters are calculated by fitting surface coverage values with functions of inhibitor concentrations. The best fit with a good correlation coefficient was showed by the Langmuir adsorption isotherm model compare to other isotherms. According to Langmuir adsorption

Fig. 6. Plot of $\ln K_{\text{ads}}$ versus $1/T$.

isotherm, θ is related to the C and K_{ads} (equilibrium constant of adsorption), using eq. (7), and K_{ads} and Gibbs free energy are related using Eq. (8)

$$\frac{C}{\theta} = \frac{1}{K_{\text{ads}}} + c \quad (7)$$

$$K_{\text{ads}} = \frac{1}{55.5} \exp\left(\frac{-\Delta G_{\text{ads}}}{RT}\right) \quad (8)$$

where C is inhibitors concentration, K_{ads} is adsorption equilibrium constant, θ is the surface coverage, T is absolute temperature, R is the universal gas constant, and 55.5 is the molar concentration of water. The Langmuir plots for IM_1 , IM_2 and IM_3 are presented in (Fig. 5a, b & 5c). The correlation coefficient values are very close to 1 indicating strong agreement with the Langmuir adsorption isotherm model. The calculated thermodynamic adsorption parameters are given in Table 6. The obtained values reveal that the K_{ads} values follow the order $\text{IM}_1 > \text{IM}_2 > \text{IM}_3$ supporting strong adsorption and greater inhibition efficiency of IM_1 compare to other imidazole derivatives. The greater adsorption of the studied imidazole derivatives is may due to interaction of nitrogen atoms of the imidazole, dimethoxy groups and pi electrons of the inhibitor and MS surface. On increasing temperature, the values of K_{ads} decreased, which explains the increase in solution entropy leads to desorption of inhibitor molecules [40]. The larger values of K_{ads} point out strong adsorption of IM_1 , IM_2 and IM_3 on the surface of MS. The negative sign of ΔG_{ads} (Table 6) reflects in the spontaneity of the adsorption process. The calculated ΔG_{ads} values of IM_1 , IM_2 and IM_3 are (-33 to 36 KJ mol^{-1}) once again representing the mixed type of adsorption i.e. involving both physisorption and chemisorption [41]. The enthalpy and entropy of adsorption (ΔH_{ads} and ΔS_{ads}) are calculated using eq. (9):

$$\ln K_{\text{ads}} = \ln \frac{1}{55.5} - \frac{\Delta H_{\text{ads}}}{RT} + \frac{\Delta S_{\text{ads}}}{R} \quad (9)$$

The evaluated values of ΔH_{ads} and ΔS_{ads} are given in Fig. 6. The negative values of ΔH_{ads} (Table 6) indicate the exothermic nature of the adsorption on the MS surface, further, the positive values of ΔS_{ads} indicate an increase in solvent entropy during adsorption [42]. The increase of disorders on MS surface is because of the elimination of a large number of water for the adsorption of one inhibitor molecules [43].

3.6. QC calculations

In order to understand the geometrical confinement of the imidazole derivatives, Gaussian 09 package with DFT calculations using B3LYP functional with 6-311 + G (d,p) level basis set for all atoms [44–46]. The optimized structures, highest occupied molecular orbitals (HOMO) and lowest unoccupied molecular orbitals (LUMO), electrostatic potential map of neutral and protonated forms of IM_1 , IM_2 and IM_3 were displayed in Fig. 7 and Fig. 8. All the calculated quantum chemical parameters such as E_{HOMO} , E_{LUMO} , electronegativity (χ), dipole moment (μ), global hardness (η), energy gap (ΔE), global softness (s), and electrophilicity index (ω) of the IM_1 , IM_2 and IM_3 and their protonated forms are shown in Table 7. Inspection of Fig. 7 revealed that HOMO density of all the studied imidazole derivatives was located on both imidazole and bis-methoxy benzene moiety indicating the major portion of the investigated imidazole derivatives were involved for electron donation [47], means the studied imidazole derivatives interact with both the cathodic and anodic sites on the metal surface through almost all parts of the inhibitors. Whereas LUMO is located on imidazole moiety and part of the bis methoxy benzene moiety. The LUMO and HOMO energy associated with electron-accepting and electron-donating capacity of the organic inhibitor molecules [48]. The reported values in Table 7 disclose that the higher HOMO value of IM_1 compares to IM_2 and IM_3 suggesting greater inhibition efficiency of IM_1 . The energy gap gives an idea in understanding the reactivity of the inhibitors. The lower the value of ΔE exhibits more reactivity of the inhibitor molecules and exerts greater inhibiting action [49]. The order of the ΔE values is $\text{IM}_1 < \text{IM}_2 < \text{IM}_3$. This order indicated that IM_1 is the best inhibitor compare to other imidazole derivatives and represents a very good correlation with the experimental results.

The electrode surface characteristics are greatly affected by the adsorption of inhibitor molecules on the surface of MS because of its dipole moment (μ). The dipole moment indicates the mechanism of inhibition of inhibitors [50]. The inhibitors with higher μ undergo greater polarization compare to inhibitors with lesser μ [51]. Therefore, the larger μ value of IM_1 (3.56) compares to IM_2 and IM_3 suggests higher corrosion inhibition performance of IM_1 . Chemical hardness (η) is also an important parameter used to predict corrosion inhibition efficiency with the experimental results. The chemical hardness and inhibition efficiency are inversely related [52]. According to Koopman's definition another parameter global softness is the inverse of global hardness. Generally, the most preferred interaction is between lowered hardness and higher softness. The hard base and soft acid theory is the basis to consider iron as soft acid and always shows a tendency to react with soft base. The

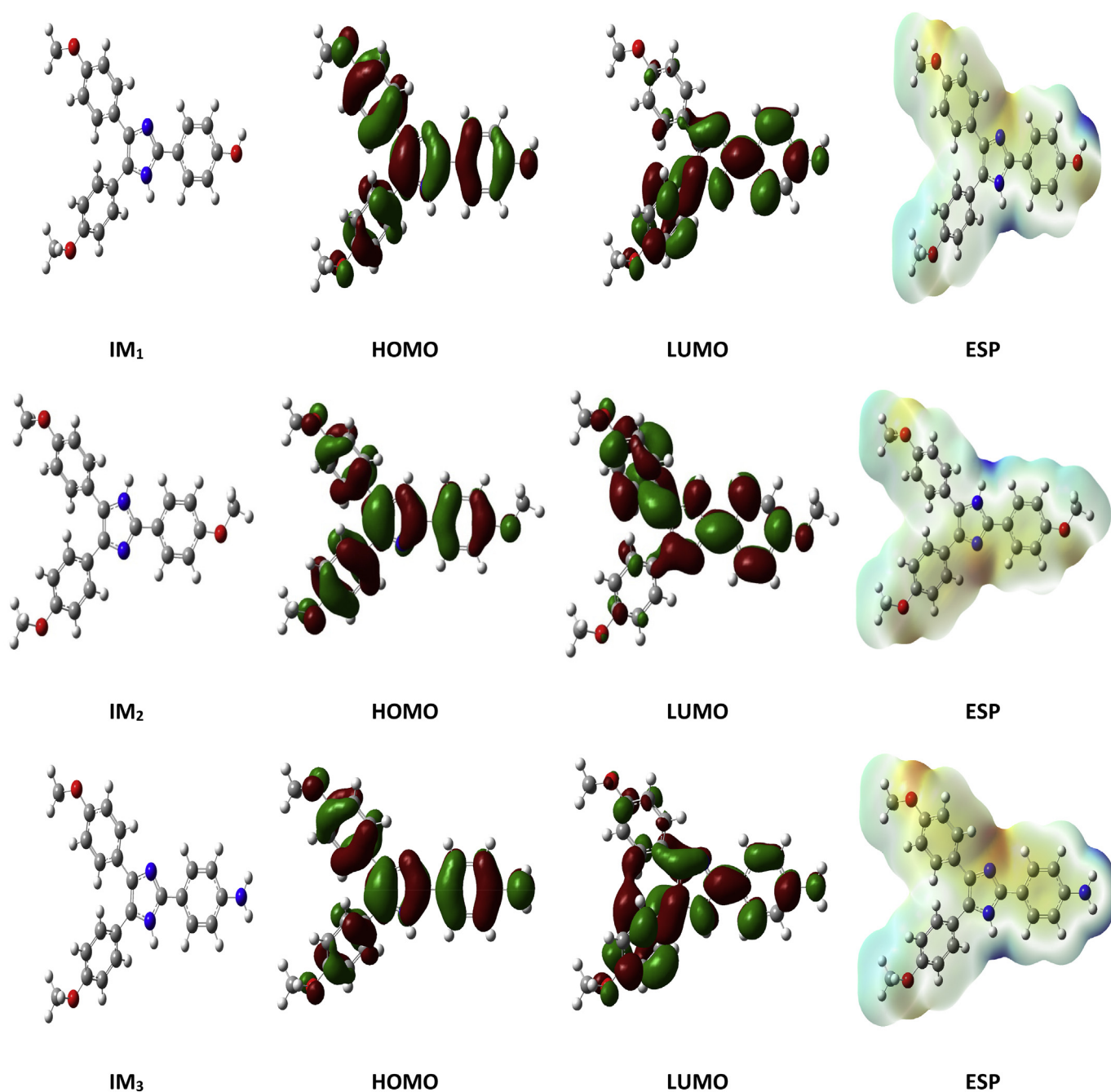


Fig. 7. The optimized structures, HOMOs, LUMOs and electrostatic potential structures of imidazole derivatives.

reported results in Table 7 suggested that IM₂ (2.02) and IM₂ (2.01) have higher hardness values compare to IM₁ (1.9) supporting greater inhibition efficiency of IM₁. Fig. 7 presents Mulliken charge population for IM₁, IM₂ and IM₃. C1, O2, C3, C4, C5, C7, C10, N11, N13, C15, C17, O18, C20, C22, C23, O25, C26 and C28 (IM₁), C1, O2, C3, C4, C5, C7, C10, N11, N13, C15, C16, C17, O18, C19, C21, C23, C24, C25, O26, C27, C29 (IM₂) and C1, O2, C3, C4, C5, C7, C10, N11, N13, C15, N18, C20, C22, C23, O25, O26, and C28 (IM₃) are having excess negative charges. The higher corrosion inhibition efficiency of all the studied imidazole derivatives is may be due to the presence of different hetero atoms such as oxygen and nitrogen atoms. After protonation of nitrogen atom of imidazole moiety acquires positive charge and adsorbed on the MS surface (Fe²⁺) combined with chlorine atom results the formation of protective complex. This protective layer formation retard corrosion of MS to a greater extent [53].

3.7. Surface morphology studies

3.7.1. XPS analysis

Further, to evaluate the composition of film adsorbed on the surface of MS, XPS analysis has been conducted in 0.5 M Hydrochloric acid solution for IM₁ Inhibitor. The C 1 s spectrum is given in Fig. 9a and it consists of three characteristic peaks of carbon. The peak at 284.5 eV is the most intense that could be accredited to the presence of C–C, C–H and C=C in IM₁. The N 1 s spectrum in Fig. 9b exhibit two distinct peaks. The peak at 399.5 eV is attributed to the unprotonated C–N and C=N of imidazole rings present in IM₁ Inhibitor. Another peak positioned at 400.4 eV is due to the co-ordination of N atoms of IM₁ with the surface of MS and probably leads to the formation of N–Fe. The Fe 2p spectrum given in Fig. 9c exhibit a typical two peaks with ghost structure at 711.6 and 725.1 eV corresponding to Fe 2p_{3/2} and 2p_{1/2},

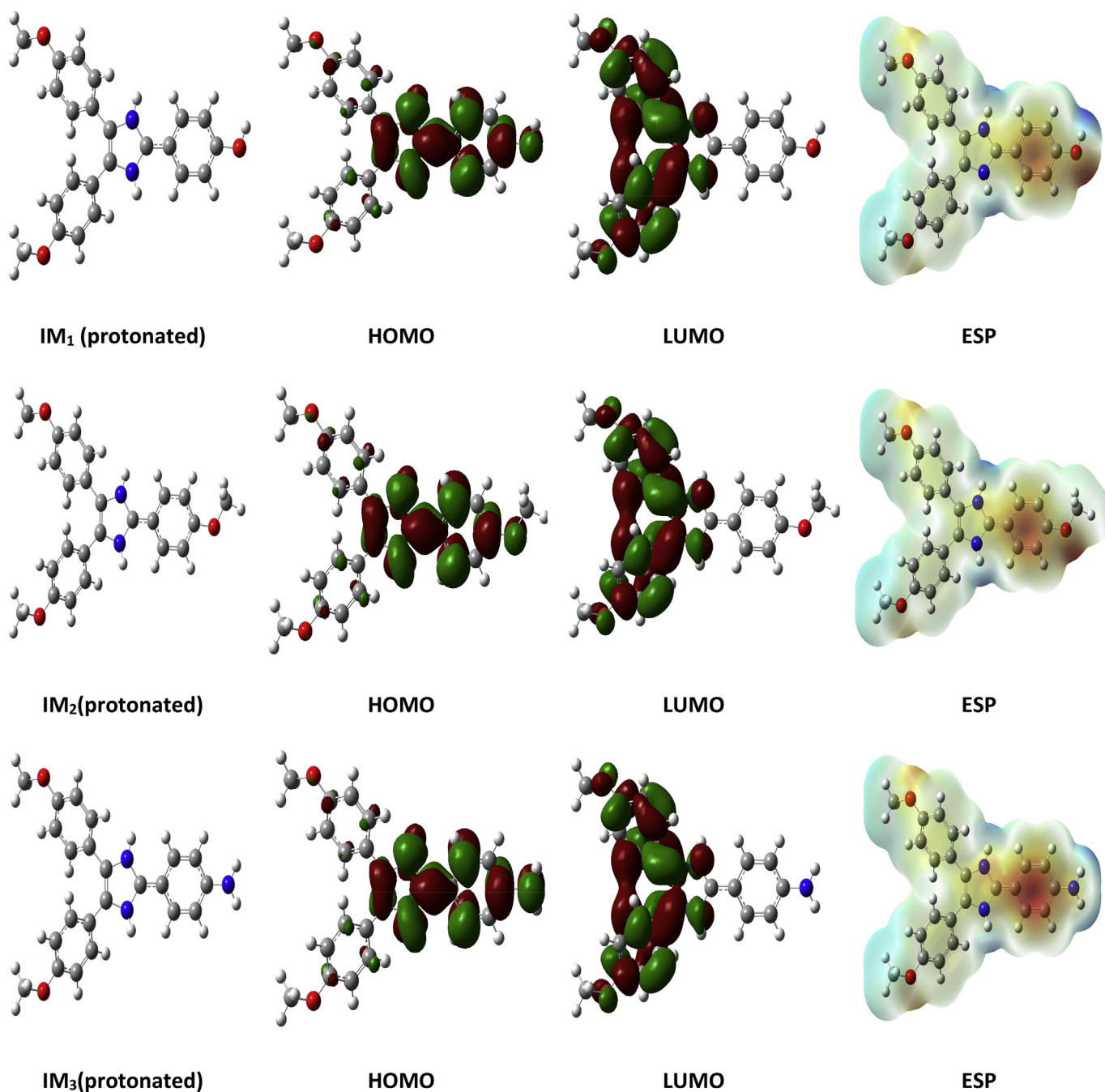


Fig. 8. The optimized structures, HOMOs, LUMOs and electrostatic potential structures of protonated imidazole derivatives.

respectively. The deconvolution of Fe 2p_{3/2} consists of four major peaks. The first peak observed at a binding energy of 710.89 eV is ascribed to Fe₂O₃ of N-Fe and a peak at 712.3 eV could be assigned to FeOOH. The other peaks at 714 and 718.75 eV are attributed to the peak of surface and satellite of Fe (III), respectively. The enhanced corrosion inhibition efficiency of IM₁ on MS in 0.5 M HCl is due to the decrease in the diffusion of ions because of generation of the Fe₂O₃ and FeOOH insoluble layer. Two main peaks are observed for O 1s (Fig. 9d), first one is at 529.95 eV attributed to oxygen atoms of Fe₂O₃ (detected in Fe 2p spectrum). The other intense peak at 531.8 eV is probably due to OH ions of FeOOH.

3.7.2. XRD analysis

Surface analysis of the MS is further evaluated using XRD studies to understand the crystalline nature of the layer adsorbed on it. To further know the crystalline nature of the layer adsorbed on the surface of MS, XRD analysis has been carried out. The surface of the MS in 0.5 M HCl in presence and absence of inhibitor was scratched and recorded the XRD. Fig. 10a exhibits characteristic peaks at $2\theta = 24.14^\circ$, 33.13° , 35.61° , 40.87° , 49.68° , 54.2° and 64.01° are attributed to the scattering from (012), (104), (110), (113), (024), (116), (214) and (300), planes respectively (JCPDS card No. 33-0664) assigned to hexagonal type α -Fe₂O₃. Fig. 10b shows the XRD of scratched samples of

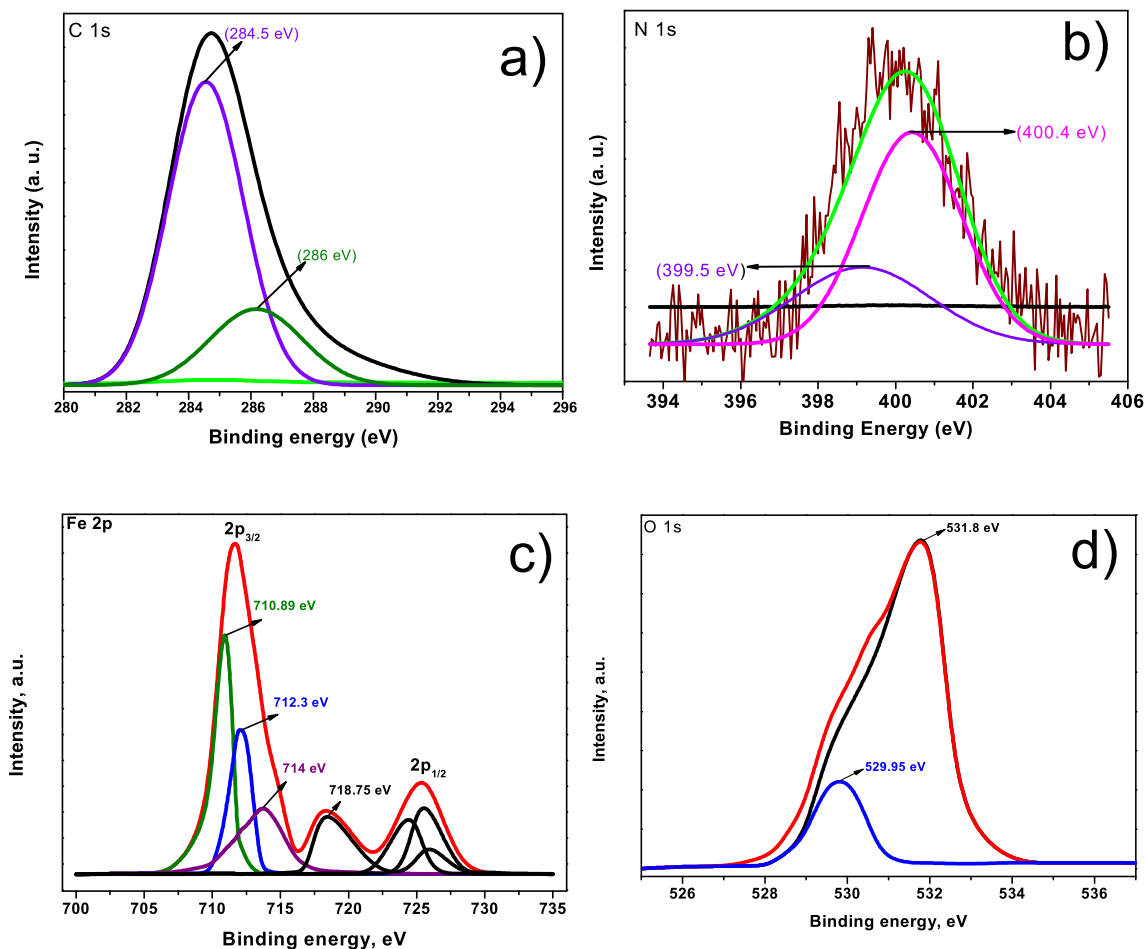


Fig. 9. XPS spectra of the MS surface after 24 h immersion in 0.5 M HCl solution uninhibited and inhibited with 0.5 mM IM₁.

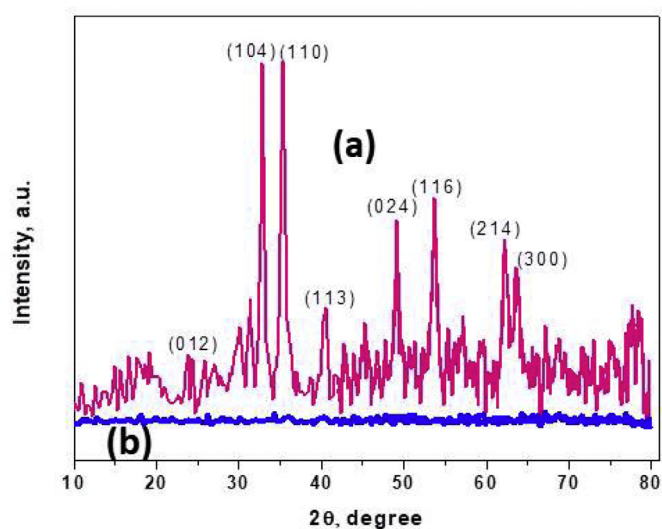


Fig. 10. XRD patterns of MS scratched sample after immersion in 0.5 M HCl and MS scratched sample after immersion in 0.5 M HCl in presence of IM₁.

MS in presence of inhibitor IM₁, clearly indicated non-crystallinity with low intensity indicated amorphous nature of the protective oxide layer.

3.7.3. Surface studies

MS surface analysis was further examined using scanning electron microscopic technique to understand the morphology of the MS in 0.5 M HCl in the absence and presence of IM₁, IM₂ and IM₃ for 24 h of immersion. Damage on the MS surface has been observed in Fig. 11a due to the dissolution of the metal in the uninhibited solution. Upon addition of the imidazole derivatives as an inhibitor to the corrosive solution, no evidence of the cracks and pits on the surface was observed in the Figs. 11(b)-11(d). These SEM images suggest a uniform surface of the MS due to the homogenous adsorption of inhibitors on its surface and indicate studied IM₁, IM₂ and IM₃ derivatives as inhibitors exhibit great affinity to adhere on MS surface.

4. Conclusions

Three imidazole derivatives have been evaluated for their corrosion inhibition efficiency on MS in 0.5 M HCl medium. The results suggest, inhibition efficiencies of all the inhibitors increase with the increase in its concentration, IM₁ with OH functional group exhibited maximum inhibition efficiency up to 96% compared to other imidazoles. Inhibition

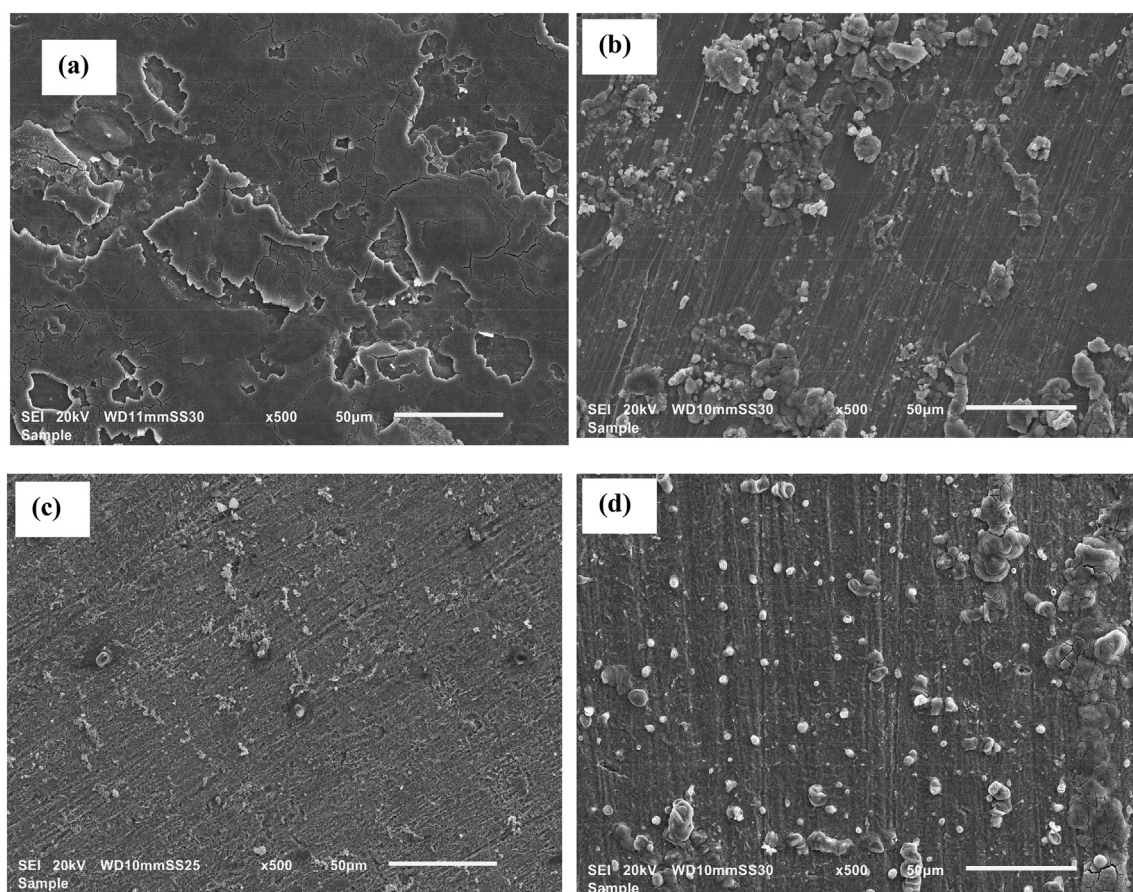


Fig. 11. SEM images of MS in 0.5 M HCl after 24 h immersion at (a) without inhibitor (blank) (b) with 1.0 mM IM₁ (c) with 1.0 mM IM₂ (d) with 1.0 mM IM₃.

Table 4

Potentiodynamic polarization parameters for MS in 0.5 M HCl in the absence and presence of different concentrations of IM₁, IM₂ and IM₃.

Inhibitor	C (mM)	E_{corr} (mV)	I_{corr} ($\mu\text{A cm}^{-2}$)	β_a (mA dec^{-1})	$-\beta_c$ (mA dec^{-1})	η (%)
IM ₁	0	-0.588 ± 0.31	766 ± 0.20	5.34 ± 0.25	7.15 ± 0.16	
	0.4	-0.549 ± 0.52	53 ± 0.21	8.70 ± 0.29	13.4 ± 0.19	93.0
	0.6	-0.556 ± 0.46	46 ± 0.20	6.97 ± 0.23	11.8 ± 0.24	93.9
	0.8	-0.557 ± 0.23	40 ± 0.19	7.30 ± 0.34	11.9 ± 0.21	94.7
	1.0	-0.528 ± 0.44	31 ± 0.20	8.42 ± 0.29	13.9 ± 0.20	95.9
IM ₂	0.4	-0.565 ± 0.28	69 ± 0.32	4.45 ± 0.15	11.1 ± 0.27	90.9
	0.6	-0.568 ± 0.30	62 ± 0.31	5.34 ± 0.19	11.6 ± 0.21	91.8
	0.8	-0.539 ± 0.24	51 ± 0.34	11.2 ± 0.11	14.3 ± 0.15	93.3
	1.0	-0.545 ± 0.26	42 ± 0.26	10.74 ± 0.34	14.8 ± 0.23	94.5
	IM ₃	0.4	-0.569 ± 0.36	78 ± 0.19	5.53 ± 0.32	12.6 ± 0.16
0.6		-0.568 ± 0.31	70 ± 0.23	6.15 ± 0.17	10.1 ± 0.15	90.8
0.8		-0.550 ± 0.30	54 ± 0.22	8.44 ± 0.22	13.9 ± 0.21	92.9
1.0		-0.524 ± 0.21	49 ± 0.21	11.84 ± 0.26	10.29 ± 0.25	93.6

efficiencies obtained by different electrochemical and weight loss methods are in good agreement with each other, inhibition efficiencies trend follows the order $\text{IM}_1 > \text{IM}_2 > \text{IM}_3$. The mechanism of adsorption of all the imidazoles follows the Langmuir isotherm model. A mixed type of corrosion inhibition activity was indicated by polarization studies. R_p values in EIS measurements increase with increasing inhibitor concentrations. SEM, XRD and XPS analysis was used to investigate the protective layer formed on the MS surface. Finally, experimental results are well correlated theoretically by using the DFT method.

Author statement

On behalf of all the coauthors am declaring that this manuscript is original, has not been published before and is not currently being considered for publication elsewhere. I confirm that the manuscript has been read and approved by all named authors and that there are no other persons who satisfied the criteria for authorship but are not listed. I further confirm that the order of authors listed in the manuscript has been approved by all of us.

Declaration of Competing Interest

All authors have participated in (a) conception and design, or analysis and interpretation of the data; (b) drafting the article or revising it critically for important intellectual content; and (c) approval of the final version.

Table 5

Weight loss data of MS in 0.5 M HCl for various concentrations of IM₁, IM₂ and IM₃ at 303 K.

Inhibitor	Concentration (mM)	Corrosion rate (mg cm ⁻² h ⁻¹)	η (%)
Blank		0.4283 ± 1.10	
4,4'-dimethoxybenzil	1.0	0.1462 ± 1.22	65
4- hydroxy benzaldehyde	1.0	0.2955 ± 1.76	31
4- methoxy benzaldehyde	1.0	0.3055 ± 0.83	28
4- Amino benzaldehyde	1.0	0.3088 ± 0.91	27
IM ₁	0.4	0.0467 ± 0.98	93
	0.6	0.0805 ± 1.10	94
	0.8	0.0322 ± 0.94	95
	1.0	0.0372 ± 1.23	96
IM ₂	0.4	0.0255 ± 0.83	90
	0.6	0.0459 ± 0.86	92
	0.8	0.0343 ± 1.32	92
	1.0	0.0434 ± 0.97	94
IM ₃	0.4	0.0546 ± 0.88	88
	0.6	0.1192 ± 0.76	89
	0.8	0.0752 ± 0.72	90
	1.0	0.1512 ± 0.92	92

Table 6

Thermodynamic parameters of adsorption for MS in 0.5 M HCl at different temperatures from Langmuir adsorption isotherm.

Inhibitor	Temperature (K)	K _{ads} (L mol ⁻¹)	ΔG _{ads} (kJ mol ⁻¹)	ΔH _{ads} (kJ mol ⁻¹)	ΔS _{ads} (J mol ⁻¹ K ⁻¹)
IM ₁	303	26,010	-33.9	-8.1	82
	313	23,420	-34.5		
	323	21,611	-35.5		
	333	20,121	-36.1		
IM ₂	303	22,121	-33.2	-8.6	83
	313	20,100	-34.5		
	323	17,221	-35.3		
	333	15,844	-36.0		
IM ₃	303	21,312	-33.6	-11.1	71
	313	19,721	-34.4		
	323	17,644	-35.1		
	333	13,492	-36.8		

Table 7

Quantum chemical parameters for neutral and protonated IM₁, IM₂ and IM₃.

Molecular Properties	Neutral			Protonated		
	IM ₁	IM ₂	IM ₃	IM ₁	IM ₂	IM ₃
E _{HOMO} (eV)	-4.9111	-5.1963	-5.1400	-2.0341	-2.3021	-2.3211
E _{LUMO} (eV)	-0.9334	-1.1562	-1.1162	-0.7796	-0.7687	-0.6555
E _{HOMO} - E _{LUMO} gap (eV)	3.9778	4.0401	4.0238	1.3785	1.5334	1.5415
Ionization Potential (I) (eV)	4.9111	5.1963	5.1400	2.3211	2.3021	2.0341
Electron affinity (A) (eV)	0.9334	1.1562	1.1162	0.7796	0.7687	0.6555
Global hardness (η)	1.9889	2.0201	2.0119	0.6893	0.7667	0.7708
Global Softness (S)	0.9944	1.0100	1.0059	0.3446	0.3833	0.3854
Chemical potential (μ)	-2.9223	-3.1763	-3.1281	1.5504	1.5354	1.3448
Electro negativity (χ)	2.9223	3.1763	3.1281	-1.5504	-1.5354	-1.3448
Electrophilicity index (ω)	2.1468	2.4971	2.4318	1.5593	1.5375	1.3119
Dipole moment (μ)	3.56	3.25	3.21	6.22	5.83	2.98

This manuscript has not been submitted to, nor is under review at, another journal or other publishing venue.

The authors have no affiliation with any organization with a direct or indirect financial interest in the subject matter discussed in the manuscript

References

- [1] E. Kusmierik, E. Chrzescijanska, Atmospheric corrosion of metals in industrial city environment, Data Brief 3 (2015) 149–154.
- [2] D. Balgude, A. Sabnis, Sol-gel derived hybrid coatings as an environment friendly surface treatment for corrosion protection of metals and their alloys, J. Sol-Gel Sci. Tech. 64 (2012) 124–134.
- [3] A.A. Nazeer, M. Madkour, Potential use of smart coatings for corrosion protection of metals and alloys: a review, J. Mol. Liq. 253 (2018) 11–22.
- [4] S. Pareek, D. Jain, S. Hussain, A. Biswas, R. Shrivastava, S.K. Parida, H.K. Kisan, H. Lgaz, I.-M. Chung, D. Behera, A new insight into corrosion inhibition mechanism of copper in aerated 3.5 wt.% NaCl solution by eco-friendly Imidazopyrimidine dye: experimental and theoretical approach, Chem. Eng. J. 358 (2019) 725–742.
- [5] C.B. Pradeep Kumar, M.K. Prashanth, K.N. Mohana, M.B. Jagadeesha, M.S. Raghu, N.K. Lokanath, K. Yogesh Kumar, Protection of mild steel corrosion by three new Quinazoline derivatives: experimental and DFT studies, Surf. Interfaces 18 (2020), 100446, .
- [6] C.B. Pradeep Kumar, K.N. Mohana, M.S. Raghu, M.B. Jagadeesha, M.K. Prashanth, N.K. Lokanath, Mahesha, "fluorine substituted thiomethyl pyrimidine derivatives as efficient inhibitors for mild steel corrosion in hydrochloric acid solution: thermodynamic, electrochemical and DFT studies", J. Mol. Liq. 113311 (2020).
- [7] C.B. Pradeep Kumar, K.N. Mohana, Corrosion inhibition efficiency and adsorption characteristics of some Schiff bases at mild steel/hydrochloric acid interface, J. Taiwan Inst. Chem. Eng. 45 (2014) 1031–1042.
- [8] V. Kalia, P. Kumar, S. Kumar, P. Pahuja, G. Jhaa, S. Lata, H. Dahiya, Synthesized oxadiazole derivatives as benign agents for controlling mild steel dissolution: experimental and theoretical approach, J. Mol. Liq. 313 (2020) 113601.
- [9] T. Nesakumar, J.I. Edison, R. Atchudan, A. Pugazhendhi, Y. Rok Lee, M.G. Sethuraman, Corrosion inhibition performance of spermidine on mild steel in acid media, J. Mol. Liq. 264 (2018) 483–489.
- [10] J.O. Mendes, E.C. da Silva, A.B. Rocha, On the nature of inhibition performance of imidazole on iron surface, Corros. Sci. 57 (2012) 254–259.
- [11] A. Popova, M. Christov, S. Raicheva, E. Sokolova, Adsorption and inhibitive properties of benzimidazole derivatives in acid mild steel corrosion, Corros. Sci. 46 (2004) 1333–1350.
- [12] S. Varvara, L.M. Muresan, K. Rahmouni, H. Takenouti, Evaluation of some non-toxic thiadiazole derivatives as bronze corrosion inhibitors in aqueous solution, Corros. Sci. 50 (2008) 2596–2604.
- [13] M. Ouakki, M. Rbaa, M. Galai, B. Lakhrissi, E.H. Rifi, M. Cherkaoui, Experimental and quantum chemical investigation of imidazole derivatives as corrosion inhibitors on mild steel in 1.0 M hydrochloric acid, J. Bio. Tribo Corros. 4 (2018) 35.
- [14] V. Srivastava, M. Salman, D.S. Chauhan, S. Abdelaizeim, M.A. Quraishi, (E)-2-styryl-1H-benzod[j]imidazole as novel green corrosion inhibitor for carbon steel: experimental and computational approach, J. Mol. Liq. 324 (2020), 115010, .
- [15] M. Ouakki, M. Galai, M. Rbaa, Ashraf S. Abousalem, B. Lakhrissi, M. EbnTouhami, M. Cherkaoui, Electrochemical, thermodynamic and theoretical studies of some imidazole derivatives compounds as acid corrosion inhibitors for mild steel, J. Mol. Liq. 319 (2020), 114063, .
- [16] M. Talari, S.M. Nezhad, S.J. Alavi, M. Mohtashampour, A. Davoodi, S. Hosseinpour, Experimental and computational chemistry studies of two imidazole-based compounds as corrosion inhibitors for mild steel in HCl solution, J. Mol. Liq. 286 (2019) 110915.
- [17] M. Ouakki, M. Rbaa, M.B. Lakhrissi Galai, E.H. Rifi, M. Cherkaoui, Experimental and quantum chemical investigation of imidazole derivatives as corrosion inhibitors on mild steel in 1.0 M hydrochloric acid, J. Bio. Tribo Corros. 4 (2018) 35.

- [18] M. Ouakki, M. Galai Rbaa, M. Ashraf, S. Abousalem, B. Lakhrissi, E.H. Rifi, M. Cherkaoui, Investigation of imidazole derivatives as corrosion inhibitors for mild steel in sulfuric acidic environment: experimental and theoretical studies, *Ionic* 26 (2020) 5251.
- [19] N.S. Patel, S. Jauhari, G.N. Mehta, The inhibition of mild steel corrosion in 1 n hcl by imidazole derivatives, *Acta Chim. Slov.* 57 (2010) 497.
- [20] U. Eduok, O. Faye, J. Szpunar, Corrosion inhibition of X70 sheets by a film-forming imidazole derivative at acidic pH, *RSC Adv.* 6 (2016), 108777, .
- [21] T. Yan, S. Zhang, L. Feng, Y. Qiang, L. Lu, D. Fu, Y. Wen, J. Chen, W. Li, B. Tan, Investigation of imidazole derivatives as corrosion inhibitors of copper in sulfuric acid: combination of experimental and theoretical researches, *J. Taiwan Inst. Chem. Eng.* 106 (2020) 118.
- [22] T. Yan, S. Zhang, L. Feng, Y. Qiang, L. Lu, D. Fu, Y. Wen, J. Chen, W. Li, B. Tan, Investigation of imidazole derivatives as corrosion inhibitors of copper in sulfuric acid: combination of experimental and theoretical researches, *J. Taiwan Inst. Chem. Eng.* 106 (2019) 118–129.
- [23] U. Eduok, O. Faye, J. Szpunar, Corrosion inhibition of X70 sheets by a film-forming imidazole derivative at acidic pH, *RSC Adv.* 6 (2016) 108777.
- [24] A. Shaabani, A.J. Rahmati, Silica sulfuric acid as an efficient and recoverable catalyst for the synthesis of trisubstituted imidazoles, *J. Mol. Catal. A Chem.* 249 (2006) 246–248.
- [25] B. Karami, K. Eskandari, A. Ghasemi, Facile and rapid synthesis of some novel polysubstituted imidazoles by employing magnetic Fe₃O₄ nanoparticles as a high efficient catalyst, *Croat. Chem. Acta* 36 (2012) 601.
- [26] A. Teimouri, A.N. Chermahini, An efficient and one-pot synthesis of 2,4,5-trisubstituted and 1,2,4,5-tetrasubstituted imidazoles catalyzed via solid acid nano-catalyst, *J. Mol. Catal. A Chem.* 46 (2011) 39–45.
- [27] A.R. Khosropour, Ultrasound-promoted greener synthesis of 2,4,5-trisubstituted imidazoles catalyzed by Zr(acac)₄ under ambient conditions, *Ultrason. Sonochem.* 15 (2008) 659–664.
- [28] M.S. Raghu, C.B. Pradeep Kumar, K.N.N. Prasad, S. Chandrasekhar, K. Yogesh Kumar, M.K. Prashanth, B. Veeresh, MoS₂-CA4 catalyzed synthesis and molecular docking study of 2,4,5-trisubstituted imidazoles as potent inhibitors of *Mycobacterium tuberculosis*, *ACS Comb. Sci.* 22 (2020) 509–518.
- [29] C. Gabrielli, Identification of Electrochemical Processes by Frequency Response Analysis: Technical Report Number 004/83, Schlumberger Instruments, 1984.
- [30] S.F. Mertens, C. Xhoffer, B.C. De Cooman, E. Temmerman, Short-term deterioration of polymer-coated 55% Al-Zn — part 1: behavior of thin polymer films, *Corrosion.* 53 (1997) 381–388.
- [31] G. Trabaneli, C. Monticelli, V. Grassi, A. Frignani, Electrochemical study on inhibitors of rebar corrosion in carbonated concrete, *Cem. Concr. Res.* 35 (2005) 1804–1813.
- [32] S.K. Shukla, M.A. Quraishi, Cefotaxime sodium: a new and efficient corrosion inhibitor for mild steel in hydrochloric acid solution, *Corros. Sci.* 51 (2009) 1007–1011.
- [33] W.R. Fawcett, Z. Kováčová, A.J. Motheo, C.A. Foss, Application of the ac admittance technique to double-layer studies on polycrystalline gold electrodes, *J. Electroanal. Chem.* 326 (1992) 91–103.
- [34] C. Verma, A.A. Sorour, E.E. Ebenso, M.A. Quraishi, Inhibition performance of three naphthyridine derivatives for mild steel corrosion in 1M HCl: computation and experimental analyses, *Results Phys.* 10 (2018) 504–511.
- [35] A. Doner, E.A. Sahin, G. Kardas, O. Serindag, Investigation of corrosion inhibition effect of 3-[(2-hydroxy-benzylidene)-amino]-2-thioxo-thiazolidin-4-one on corrosion of mild steel in the acidic medium, *Corros. Sci.* 66 (2013) 278–284.
- [36] A. Dehghani, G. Bahlakeh, B. Ramezanzadeh, M. Ramezanzadeh, Detailed macro-/micro-scale exploration of the excellent active corrosion inhibition of a novel environmentally friendly green inhibitor for carbon steel in acidic environments, *J. Taiwan Inst. Chem. Eng.* 100 (2019) 239–261.
- [37] C. Verma, E.E. Ebenso, M.A. Quraishi, Molecular structural aspects of organic corrosion inhibitors: influence of –CN and –NO₂ substituents on designing of potential corrosion inhibitors for aqueous media, *J. Mol. Liq.* 255 (2020) 113874.
- [38] C.B. Pradeep Kumar, K.N. Mohana, Phytochemical screening and corrosion inhibitive behavior of *Pterolobium hexapetalum* and *Celosia argentea* plant extracts on mild steel in industrial water medium, *Egypt. J. Pet.* 23 (2014) 201–211.
- [39] A. Singh, K.R. Ansari, D.S. Chauhan, M.A. Quraishi, H. Lgaz, Comprehensive investigation of steel corrosion inhibition at macro/micro level by ecofriendly green corrosion inhibitor in 15% HCl medium, *J. Colloid Interface Sci.* 560 (2020) 225–236.
- [40] L. Jiang, Y. Qiang, Z. Lei, J. Wang, Z. Qin, B. Xiang, Excellent corrosion inhibition performance of novel quinoline derivatives on mild steel in HCl media: experimental and computational investigations, *J. Mol. Liq.* 255 (2018) 53–63.
- [41] R. Solmaz, G. Kardas, B. Yazıcı, M. Erbil, Adsorption and corrosion inhibitive properties of 2-amino-5-mercapto-1,3,4-thiadiazole on mild steel in hydrochloric acid media, *Colloids Surfaces A* 312 (2008) 7–17.
- [42] R.S.A. Hameed, Aminolysis of polyethylene terephthalate waste as corrosion inhibitor for carbon steel in HCl corrosive medium, *Adv. Appl. Sci. Res.* 2 (2011) 483–499.
- [43] M. Bouklah, B. Hammouti, M. Lagrenee, F. Bentiss, Thermodynamic properties of 2,5-bis(4-methoxyphenyl)-1,3,4-oxadiazole as a corrosion inhibitor for mild steel in normal sulfuric acid medium, *Corros. Sci.* 48 (2006) 2831–2842.
- [44] C. Lee, W. Yang, R.G. Parr, Development of the Colle-Salvetti correlation-energy formula into a functional of the electron density, *Phys. Rev. B* 37 (1988) 785–789.
- [45] A.D. Becke, Density-functional thermochemistry. I. the effect of the exchange-only gradient correction, *J. Chem. Phys.* 96 (1992) 2155–2160.
- [46] P.C. Hariharan, J.A. Pople, The influence of polarization functions on molecular orbital hydrogenation energies, *Theor. Chem. Accounts* 28 (1973) 213–222.
- [47] S.K. Saha, A. Dutta, P. Ghosh, D. Sukul, P. Banerjee, Novel Schiff-base molecules as efficient corrosion inhibitors for mild steel surface in 1 M HCl medium: experimental and theoretical approach, *Phys. Chem.* 18 (2016) 17898–17911.
- [48] S. Xia, M. Qiu, L. Yu, F. Liu, H. Zhao, Molecular dynamics and density functional theory study on relationship between structure of imidazoline derivatives and inhibition performance, *Corros. Sci.* 50 (2008) 2021–2029.
- [49] M. Ozcan, I. Dehri, M. Erbil, Organic Sulphur-containing compounds as corrosion inhibitors for mild steel in acidic media: correlation between inhibition efficiency and chemical structure, *Appl. Surf. Sci.* 236 (2004) 155–164.
- [50] G. Gece, The use of quantum chemical methods in corrosion inhibitor studies, *Corros. Sci.* 50 (2008) 2981–2992.
- [51] A. Mishra, C. Verma, H. Lgaz, V. Srivastava, M.A. Quraishi, E.E. Ebenso, Synthesis, characterization, and corrosion inhibition studies of *N*-phenyl-benzamides on the acidic corrosion of mild steel: experimental and computational studies, *J. Mol. Liq.* 251 (2018) 317–332.
- [52] L.O. Olasunkanmi, M.F. Sebona, E.E. Ebenso, Influence of 6-phenyl-3(2*H*)-pyridazinone and 3-chloro-6-phenylpyrazine on mild steel corrosion in 0.5 M HCl medium: experimental and theoretical studies, *J. Mol. Struct.* 1149 (2017) 549–559.
- [53] E.A. Yaqo, R.A. Anae, M.H. Abdul Majeed, I. Hameed R. Tomi, M. Mohammed Kadhim, Potentiodynamic polarization, surface analyses and computational studies of a 1,3,4-thiadiazole compound as a corrosion inhibitor for Iraqi kerosene tanks, *J. Mol. Struct.* 1202 (2020) 127356.